Ferromagnetic and insulating behavior of $LaCoO_3$ films grown on a (001) $SrTiO_3$ substrate: A simple ionic picture explained *ab initio*

Adolfo O. Fumega* and V. Pardo†

Departamento de Física Aplicada and Instituto de Investigacións Tecnolóxicas, Universidade de Santiago de Compostela, E-15782 Campus Sur s/n, Santiago de Compostela, Spain

(Received 10 April 2017; revised manuscript received 14 June 2017; published 6 October 2017)

This paper shows that the oxygen vacancies observed experimentally in thin films of $LaCoO_3$ subject to tensile strain are thermodynamically stable according to *ab initio* calculations. By using DFT calculations, we show that oxygen vacancies on the order of 6% forming chains perpendicular to the (001) direction are more stable than the stoichiometric solution. These lead to magnetic Co^{2+} ions surrounding the vacancies that couple ferromagnetically. The remaining Co^{3+} cations in an octahedral environment are nonmagnetic. The gap leading to a ferromagnetic insulating phase occurs naturally and we provide a simple ionic picture to explain the resulting electronic structure.

DOI: 10.1103/PhysRevMaterials.1.054403

I. INTRODUCTION

Ferromagnetic insulators (FMI) and in particular ferromagnetic oxides are uncommon materials. The usual situation is that a ferromagnetic coupling occurs together with metallic behavior. In the case of oxides, the most common situation for insulators is that they order antiferromagnetically. However, several examples of ferromagnetic insulating oxides do exist, such as spinels [1,2], perovskite-based $La_{1-x}Sr_xMnO_3$ [3], La_2CoMnO_6 [4], etc. These are of extreme importance in the fabrication of spintronic devices [5–8]. Due to their technological relevance and rarity, it is interesting to explore and clarify the properties of one of such systems since this could help in designing other oxides with improved properties.

$LaCoO_3$ (LCO) is a very intriguing insulator with a not-completely understood spin-state transition [9–14], and also an interesting excitonic behavior [15]. In its bulk form it presents a diamagnetic response at low temperatures, all the Co^{3+} cations being in a nonmagnetic low-spin state, with all of its six electrons occupying the lower-lying t_{2g} levels. As temperature rises, a crossover to other spin states occurs leading to an increase in the magnetic susceptibility [16]. However, when LCO is grown as a thin film on a substrate that induces epitaxial strain on it, a ferromagnetic phase appears at low temperatures, characterized by a saturation magnetization close to 0.8 μ_B/Co, in case the substrate is $SrTiO_3$ (STO), and a T_c of about 80 K [17–21]. Early explanations [17–19,22,23] discussed this magnetic ordering as arising in a stoichiometric strained form of LCO from a spin-state ordering formed by a Co^{3+} HS-LS alternating pattern. However, more recent experiments have shown that epitaxial strain induces the formation of oxygen vacancy planes. The off-stoichiometry changes the electron count and leads to magnetic moments on some Co atoms and these eventually couple ferromagnetically [20,24–26].

In Ref. [24] a combination of atomically resolved *Z*-contrast imaging and electron-energy-loss spectroscopy is used to prove that, when LCO is grown on STO (001), oxygen vacancy planes are formed perpendicular to the substrate with a repetition of one vacancy plane every three unit cells. This pattern has also been interpreted as coming from a kind of spin-state ordering providing the contrast [27].

Taking those images as a basis for our calculations, here we present a DFT study on the possible oxygen-vacancy configurations consistent with the *Z*-contrast imaging pictures published by various groups in different samples, grown by physical methods such as pulsed laser deposition [20,24] or by chemical methods such as polymer assisted deposition [21] that could account for the ferromagnetic insulating behavior found experimentally.

Our total energy calculations in the various possible configurations allow us to understand the amount of vacancies that are stable, what environments for the neighboring cations these produce, how the local moments couple, and the resulting electronic structure. Thus, our work helps clarifying the origin of the insulating behavior found in these thin films.

II. COMPUTATIONAL PROCEDURES

Ab initio electronic structure calculations based on density functional theory (DFT) [28,29] have been performed using an all-electron full potential code (WIEN2K [30]) on LCO. The exchange-correlation term is parametrized depending on the case.

We have used the generalized gradient approximation (GGA) in the Perdew-Burke-Ernzerhof [31] scheme for structural optimizations and to compute the energetics of the different configurations of LCO. These calculations were performed with a converged *k* mesh and a value of $R_{mt}K_{max} = 5.0$. The R_{mt} values used were in a.u.: 1.80 for La, 1.40 for Co, and 1.11 for O when studying LCO energetics. The need to compare energetics considering the O_2 molecule explains the choice of such small R_{mt} values. In order to compute the energy of the O_2 molecule, an fcc lattice was used with the molecule at the center and a large enough unit cell so the bond length is converged and it gives a value of 1.20 Å, which compares reasonably well with the experimental O-O bond length of 1.21 Å [32].

*adolfo.otero@rai.usc.es
†victor.pardo@usc.es

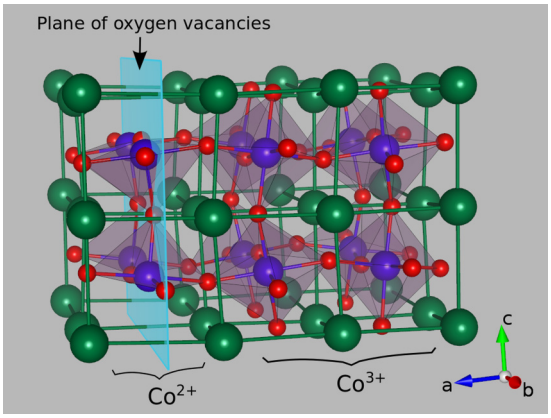

FIG. 1. Unit cell representation of $La_{12}Co_{12}O_{36-n}$ used in the calculations. La in green, Co in purple, and O in red. The blue plane corresponds to the plane in which the oxygen vacancies are imposed. Notice that this plane is parallel to the bc plane and perpendicular to the substrate-film plane ab. In the ground state configuration, Co^{2+} cations occur in the plane of O-vacancies while the other Co atoms are Co^{3+}.

To include correlation effects in the Co d manifold, we have used the LDA+U method ($U = 7$ eV, $J = 0.7$ eV) in order to find a good description of the magnetic moments of the Co cations, their couplings, and the overall electronic structure. A mapping of U between 4 and 8 eV was carried out to determine the energy term E_e in Eq. (1). A converged k mesh and a value of $R_{mt}K_{max} = 6.0$ were used. The R_{mt} values used in that case were in a.u.: 2.33 for La, 1.83 for Co, and 1.62 for O. The atomic magnetic moment values quoted below correspond to this kind of calculation.

III. RESULTS AND DISCUSSION

We have divided the study into two main parts: structural characterization and electronic structure and magnetic properties of tetragonally strained LCO. First, we need to understand how many oxygen vacancies will appear and how they are distributed. Once the structural ground state is found, we proceed to describe the electronic structure and magnetic properties that result from that ground state configuration.

A. Structural characterization

In this section of the analysis we have characterized the structural properties of LCO when it has tetragonal symmetry and the in-plane lattice parameters are those of STO, mimicking the epitaxial strain effect introduced in an LCO film by the growth on an STO substrate. We have performed a systematic study that allows us to determine the optimal oxygen vacancy concentration as well as their distribution in the plane of vacancies. The unit cell that we have considered is shown in Fig. 1. Its stoichiometry is $La_{12}Co_{12}O_{36-n}$ where n is the number of oxygen vacancies. We have fixed the lattice parameters a and b to reproduce the in-plane strain due to STO (3.905 Å) [33]. Parameter c was left free for optimization. As Fig. 1 shows, the c direction is the (001) growth direction in the standard experiments with thin LCO films on a cubic perovskite substrate. We have allowed all the possible octahedral rotations that occur in bulk LCO and fully relaxed all the atomic coordinates.

We have introduced one plane including O vacancies out of every three La-rich planes, as it is observed in experiments, such as Ref. [20] (see Fig. 1, light blue plane). In our study, we have performed calculations for ten different oxygen-vacancy configurations, as described in Fig. 2. The number of possible configurations increases with the number of oxygen vacancies, that is one of the reasons why we stop the analysis in 2 vacancies. Also, with 3 vacancies or more we could not figure out a simple ionic model that would yield a ferromagnetic insulating state at the same time as providing a magnetic moment close to the experimental value. However, we foresee that we have found a 2-oxygen-vacancy configuration that is in agreement with the experimental data. For choosing the different configurations we have taken into account the tetragonal symmetry of the system, considering that a basal O is different than an apical one, but retaining xy symmetry for the analysis.

In order to compute the energy E of each configuration we have used the following equation [34–36]:

$$E = E_{\text{conf}} + \frac{n}{2}E_{O_2} - 2nE_e - E_{0\_\text{vac}}, \quad (1)$$

where E_{conf} is the energy of one of the configurations shown in Fig. 2 (the effect of charged vacancies is not included in this term). E_{O_2} is the energy of the O_2 molecule, calculated as described in Sec. II, and n the number of vacancies. E_e is the term that provides the energy due to the charged vacancies. It is computed as the difference in energy between the top of the valence band of the configuration that we are calculating and the top of the valence band of the configuration without vacancies (0_vac). In order to set a common zero of energies for each case, we chose the energy of an O 1s orbital of an oxygen that lies away from the vacancy plane. The factor 2 is the charge, supposing they become fully ionized, as is found in other oxides [37]. Finally, E_{0_vac} is the energy of the configuration without vacancies 0_vac, this term represents the zero of energies when obtaining E from Eq. (1). We have assumed that all the vacancies form O_2 and we have also neglected the electrostatic interaction between the homogeneous background charge and the charged vacancies. This assumption was made considering previous works [34–36] and the fact that the most stable compound for the oxygen element is the O_2 molecule.

All terms in Eq. (1) were calculated using the GGA scheme, but E_e was computed using the LDA+U scheme for various U values, since GGA leads to metallic solutions and the LDA+U method allows us to compare the band alignment between two realistic insulating solutions, both for the stoichiometric and nonstoichiometric systems.

The results for the energy of each oxygen-vacancy configuration using Eq. (1) are shown in Fig. 3. We observe that only configuration 2_vac_D is more stable than the one without vacancies. This corresponds to chains of oxygen vacancies perpendicular to the (001) and contained in the plane of vacancies (see Fig. 2).

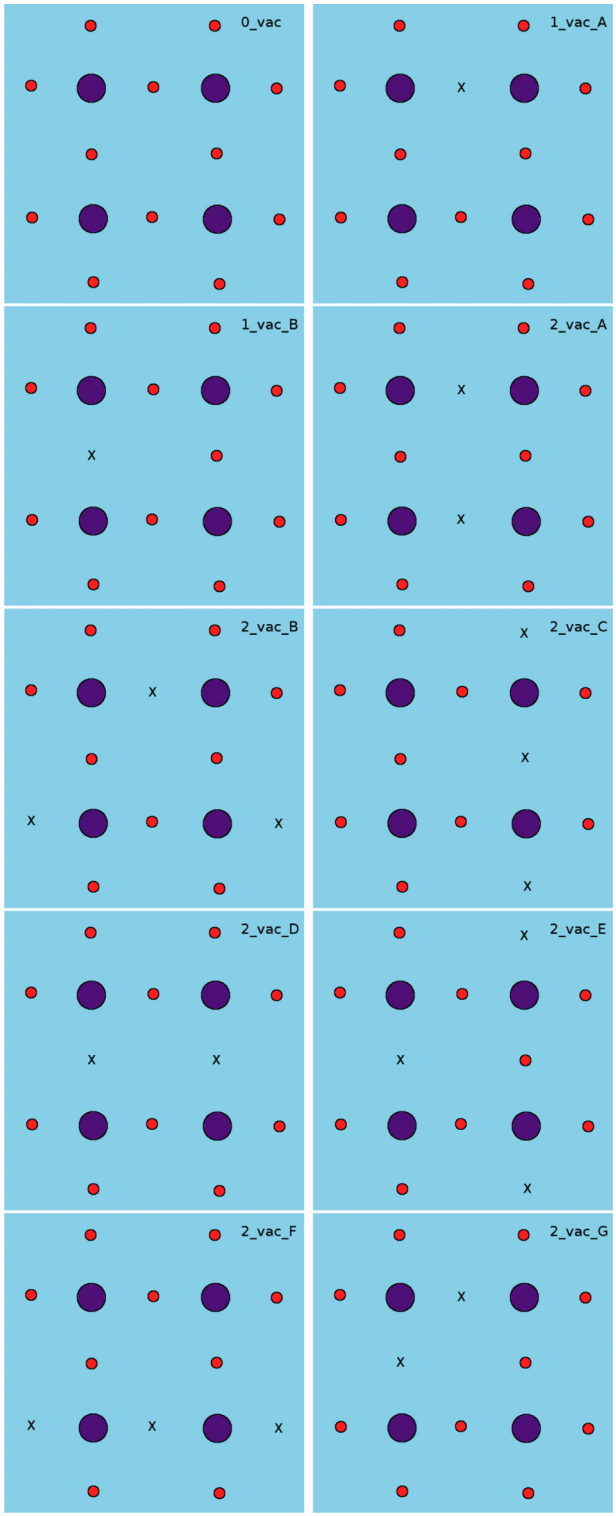

FIG. 2. Ten different oxygen-vacancy configurations, all of them projected on the blue plane described in Fig. 1. Co is in purple, O in red, and the vacancies are represented by a cross. In each panel, the O on the left-hand side are equivalent to those on the right and the bottom to the top ones. 0_vac stands for LCO without vacancies, 1_vac_A and 1_vac_B correspond to the two different possibilities when one O vacancy is introduced, 2_vac_A, 2_vac_B, 2_vac_C, 2_vac_D, 2_vac_E, 2_vac_F, and 2_vac_G are the seven 2-O-vacancy configurations. The horizontal coordinate corresponds to the b parameter and the vertical one to c.

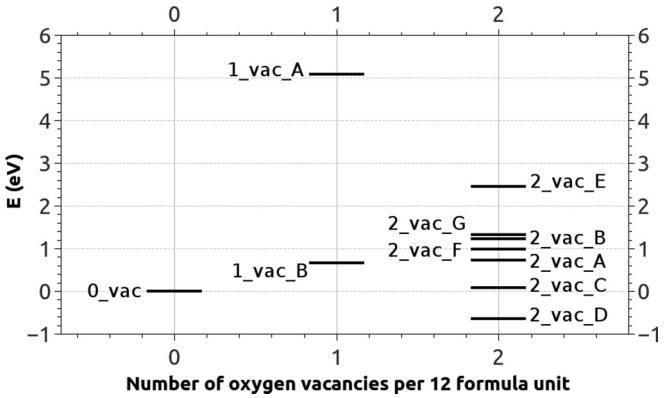

FIG. 3. Energetics for the different oxygen-vacancy configurations computed using Eq. (1). We can see that the most stable configuration is the 2_vac_D. This configuration corresponds to vacancy chains perpendicular to the (001) and contained in the vacancy plane. Only results with $U = 7$ eV are presented in this figure.

Before analyzing in detail configuration 2_vac_D, which is the ground state, we can explore the other configurations. For the case without vacancies, the system is a nonmagnetic insulator. We also see that this configuration is quite stable compared to the others that present oxygen vacancies (2_vac_D is the only configuration with vacancies that is more stable than the stoichiometric solution). If we put an eye now on the two configurations with one vacancy, we will realize that one of them is much more stable than the other. The difference in energy between them is a sizable 0.37 eV/Co. This result suggests that in the case of adding a second vacancy, it could be energetically favorable to include it in an equivalent position to configuration 1_vac_B, i.e., forming chains perpendicular to the (001) direction. We have demonstrated this statement calculating the energy for the seven possible 2-vacancy configurations. As we have said 2_vac_D gives a stable solution. All the other $n = 2$ cases are also FMI solutions, but higher in energy, except 2_vac_C, which is a ferromagnetic metal. We have tried several values of U in a wide range, but an energy gap was not opened for that particular configuration.

If we analyze in more detail the structure of the 2_vac_D configuration that we have obtained from our calculations, we find the following characteristics that can be compared with the experimental results reported in Ref. [20]. The lattice parameter along the (001) direction undergoes a contraction compared to the bulk value of LCO. We have obtained $c = 3.810$ Å, which is in reasonable agreement with the experimental value $c = 3.767$ Å [20]. The distance between LaO planes parallel to the plane of oxygen vacancies depends on whether one considers the distance between two LaO planes that contain the plane of vacancies or two stoichiometric planes. In the former case, with the plane of oxygen vacancies inside, we found that the distance is 4.02 Å. In the other case we found it is 3.85 Å. Experimentally, the same trend is observed but with a larger ratio [24].

We have found in this subsection a configuration of oxygen vacancies that agrees with the experimental microscopy data obtained for LCO films grown on STO.

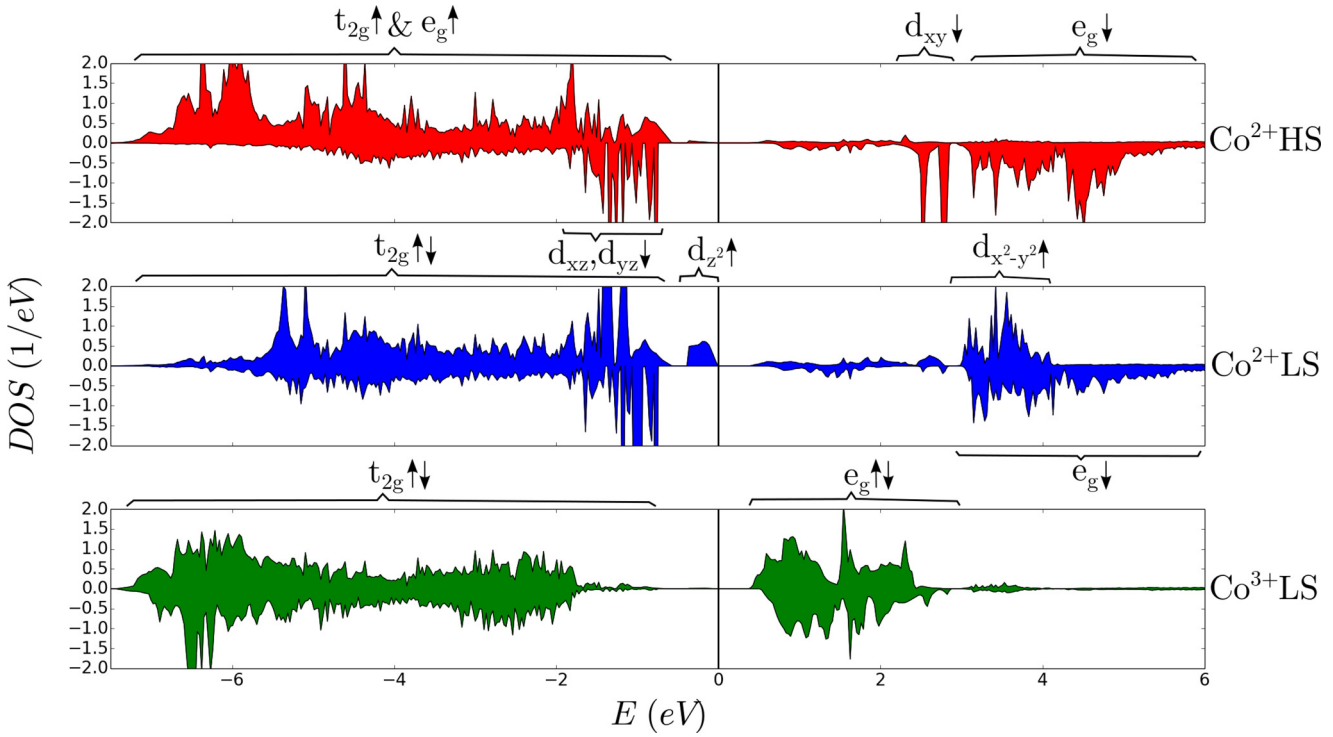

FIG. 4. Partial DOS for Co^{2+} HS, Co^{2+} LS, and Co^{3+} LS computed in the LDA+U scheme, for $U = 7$ eV. The Fermi level is set to the zero of energies. Upper panel, Co^{2+} HS: the t_{2g} and the e_g majority-spin states are occupied, and also the d_{xz},d_{yz} minority orbitals. Middle panel, Co^{2+} LS: the t_{2g} majority and minority orbitals are occupied and so is the d_{z^2} majority. Lower panel, Co^{3+} LS: the t_{2g} majority and minority orbitals are occupied.

B. Electronic structure and magnetic behavior

In this section we analyze the electronic structure of configuration 2_vac_D. As we have already said, this presents a ferromagnetic-insulator behavior and is found to be a ground state. This is confirmed by antiferromagnetic (AFM) calculations performed for this configuration (see Appendix A for more details). We will try first to explain the simple ionic model that accounts for the magnetic moments observed and its consistency with the *ab initio* calculations of the partial density of states (DOS) of the Co atoms shown in Fig. 4. In it, we can see the three types of Co atoms that appear in the converged solution: a nonmagnetic Co atom sixfold coordinated and two magnetic Co atoms with fivefold oxygen coordination, one with a higher value of the magnetic moment than the other.

From an ionic picture, if we consider the unit cell shown in Fig. 1, we have La^{3+}, O^{2-}, and Co^{3+} for the stoichiometric compound without vacancies. The t_{2g} orbitals of Co^{3+}, which are in an octahedral environment, are occupied in the low-spin (LS) state, see Fig. 5(c), which gives rise to a nonmagnetic moment and an insulating state caused by crystal-field splitting between the Co t_{2g} and e_g levels that leads to a gap opening around the Fermi level in the simple diamagnetic configuration.

If we remove now two oxygens from the unit cell (Fig. 1), we have the stoichiometry $La_{12}Co_{12}O_{34}$. Structurally, there are four Co atoms that are fivefold coordinated and the remaining eight Co cations are sixfold octahedrally coordinated and remain nonmagnetic, suggesting they retain the original 3+ valence. A simple electron count would naively imply that the other four Co atoms are Co^{2+} cations. These are in a five-oxygen environment that could be analyzed in an ionic picture as an octahedral environment distorted in the z axis.

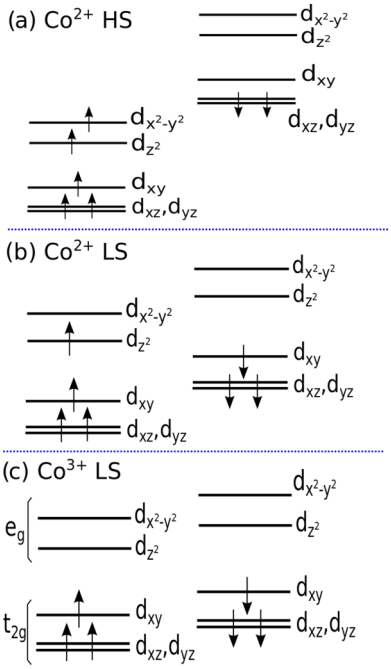

FIG. 5. Ionic model for Co^{2+} HS, Co^{2+} LS, and Co^{3+} LS. (a) Co^{2+} HS: the t_{2g} and the e_g majority states are occupied, and also the d_{xz},d_{yz} minority orbitals. (b) Co^{2+} LS: the t_{2g} majority and minority orbitals are occupied and also the d_{z^2} majority. (c) Co^{3+} LS: the t_{2g} majority and minority orbitals are occupied.

Such distortion breaks the degeneracy of the t_{2g} and the e_g levels as sketched in Fig. 5. The coordinate system that we use to analyze the electronic structure is local to each Co atom with z lying along the Co-O-vacancy direction. Our calculations show that the magnetic moment values are consistent with an ionic picture where half of these Co^{2+} cations are in the LS state (in the 2_vac_D panel of Fig. 2 the Co atoms on the left side), and the other half in the HS state (the ones on the right side). The actual values for the magnetic moments inside the muffin-tin spheres obtained from our calculations are approximately 0.8 and 2.4 μ_B, which account for the ionic values plus substantial hybridizations. Taking into account Fig. 5: for the case of Co^{2+} LS [Fig. 5(b)], we observe that the t_{2g} bands are fully occupied and there is one extra electron occupying the lower-lying e_g state, which is of d_{z^2} parentage due to the missing apical oxygen. Thus, the LS Co^{2+} cations are in an $S = 1/2$ state. In the case of Co^{2+} HS [Fig. 5(a)], the majority channel is fully occupied, i.e., the t_{2g} and the e_g majority states are occupied, there are two minority t_{2g} electrons occupying the lower-lying doublet xz/yz, which is split from the higher-lying xy orbital due to the missing apical oxygen in the fivefold-coordinated environment. This leads to $S = 3/2$ HS state. This simple ionic picture can be observed to be approximately reproduced (with substantial hybridizations, as is common in transition metal oxides) in the partial DOS for each inequivalent Co cation shown in Fig. 4. In this figure we show that the DFT calculations can be understood with the simplistic ionic model sketched in Fig. 5. The labels in Fig. 4 help us to see the correspondence with the ionic model. Spectroscopy data confirm that most of the sample is Co^{3+} nonmagnetic and that some magnetic Co^{2+} exist [20]. The data do not discard the existence of Co^{3+} HS yet they cannot confirm it. Our calculations show that Co^{3+} HS does not appear. No analysis of the possible existence of Co^{2+} LS that our calculations predict is provided in Ref. [20], thus our calculations are in principle consistent with spectroscopic evidences.

The total spin magnetic moment in this solution is 0.67 μ_B/Co. If we now include spin-orbit coupling in the calculations, the total ordered moment obtained as the sum of $l_z + 2s_z$ is about 0.8 μ_B/Co, since the magnetic Co cations present a non-negligible orbital angular momentum that becomes partially unquenched. This is in reasonable agreement with the saturation magnetization of the LCO thin films obtained experimentally of about 0.85 μ_B/Co [20].

As we have previously stated, we have performed AFM calculations of the 2_vac_D configuration. We have considered five different AFM configurations that allowed us to determine the magnetic exchange coupling at second neighbors. Their energy was computed using Eq. (1). Results show that all the magnetic exchange couplings are ferromagnetic when the total energy differences are fit to a Heisenberg model (see Appendix A for more details).

We also observe in Fig. 4 that the energy gap is between the d_{z^2} orbital of the Co^{2+} LS (top of the valence band) and the e_g of the Co^{3+} LS (bottom of the conduction band). Of course the particular value of the gap will depend on the value of U chosen for the LDA+U calculations. In particular, for the DOS presented in Fig. 4, the value used was 7 eV. According to our results, the insulating properties of these films occur

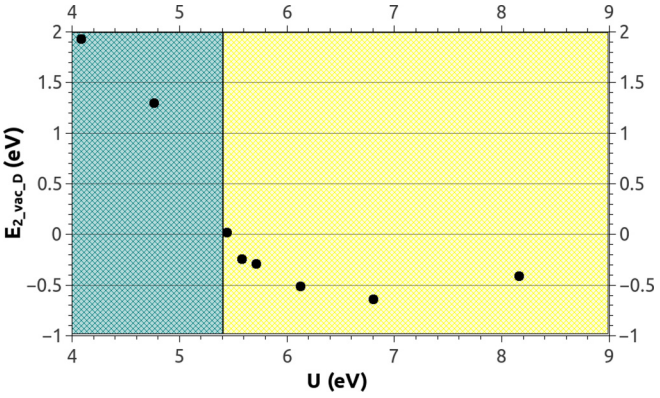

FIG. 6. Energy of the 2_vac_D configuration as a function of U computed using Eq. (1). The zero of energies would be the stoichiometric solution without vacancies. We observe that for values of $U > 5.5$ eV the configuration labeled 2_vac_D becomes stable.

naturally due to the additional band splittings introduced by nonoctahedral environments.

We have characterized in this section the electronic structure of the 2_vac_D configuration. We have related the calculated DOS to a simple ionic model that explains both the ferromagnetic ordering with a consistent value of the total magnetic moment and the insulating behavior.

C. Stabilization of the ground state configuration with U

Regarding the value of U used to compute the energies shown in Fig. 3, we have first performed calculations for different U values, and in particular Fig. 3 was presented for $U = 7$ eV. Figure 6 shows that there is a range of U values where 2_vac_D becomes stable, and such U is within that range. We have also seen that configuration 2_vac_D is a robust ground state in a wide range of U values above 5.5 eV (see Appendix B). This U value is similar to other values used in the literature for these kinds of systems [23,38,39]. We observe that for values of U less than 5.5 eV the 2_vac_D configuration is not stable. This can be analyzed through the change in the

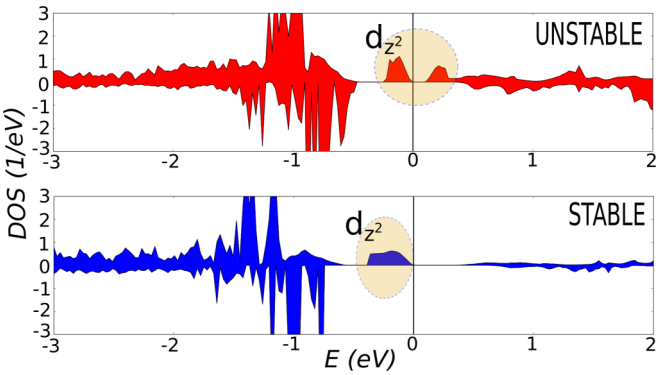

FIG. 7. Partial DOS Co^{2+} LS for two different values of U, 4 and 7 eV, respectively. Upper panel: We observe that the d_{z^2} orbital (highlighted in yellow) is not fully occupied which results in a solution that is not the ground state. Lower panel: We observe in this case that the d_{z^2} orbital is fully occupied, which stabilizes the 2_vac_D configuration to become the ground state.

electronic structure that occurs when comparing the low-U and high-U solutions. Plots of the partial DOS of Co^{2+} LS for two different values of U, one for an unstable case and another one for the stable case, are shown in Fig. 7. We can see that the d_{z^2} orbital of the Co^{2+} LS is not fully occupied for the unstable case, while it becomes totally occupied for the stable case at larger U values. This change in the electronic structure is correlated with the stabilization of the 2_vac_D configuration.

IV. CONCLUDING REMARKS

In this study we have analyzed the ferromagnetic-insulating behavior of LCO when it is grown on (001) STO. We have used DFT calculations to analyze the electronic structure properties of LCO under tensile strain and for various stoichiometries including different oxygen vacancy configurations and concentration.

We have found that the ground state of LCO when it is grown on STO is given by an off-stoichiometry of the form $LaCoO_{2.83}$ produced by about 6% oxygen vacancies. We have shown that the vacancies form chains perpendicular to the (001) direction and are contained in the plane perpendicular to the film/substrate interface, consistent with experimental findings. Other structural features like the distance between La layers or the lattice parameter in the (001) direction agree with the experimental measurements.

We found that the Co atoms that lie in the plane of vacancies are a mixture of Co^{2+} LS and Co^{2+} HS. The total magnetic moment is in close agreement with experimental measurements. The ferromagnetic insulating behavior of the film is readily obtained as a ground state, the gap opening occurring naturally in that electron count due to the appearing crystal field splittings together with the addition of a reasonable U value. Our *ab initio* total energy calculations confirm that all the nearest-neighbor magnetic exchange couplings are indeed ferromagnetic.

In conclusion, we can say that the strain introduced by STO on LCO favors the presence of O-vacancy chains perpendicular to the (001) direction. Ferromagnetism arises from the inclusion of those vacancy chains and can be explained with an ionic model. The results presented in this work could lead to a better understanding and the eventual design of other ferromagnetic-insulator oxides in which oxygen vacancies could play an important role.

ACKNOWLEDGMENT

This work has been supported by the MINECO of Spain through the project MAT2016-80762-R.

APPENDIX A

In this Appendix we summarize the AFM calculations we have carried out. The FM solution is lower in energy and hence it is the ground state.

The configurations that we have calculated to explain the FM plane in the ground state configuration 2_vac_D are the ones shown in Fig. 8. The corresponding magnetic exchange coupling constants we have introduced into a Heisenberg model of the system are depicted as the various J's. The energies of each magnetic configuration are shown in Table I. They are all referred to the energy of the ferromagnetic (FM) configuration E_{FM}, which is taken as zero. Total energy is given for the whole unit cell (12 Co atoms in total). The arrangement of the Co^{2+} HS and LS is preserved for all the magnetic configurations and the geometry of the structure is not changed. We see that the FM configuration is the most stable.

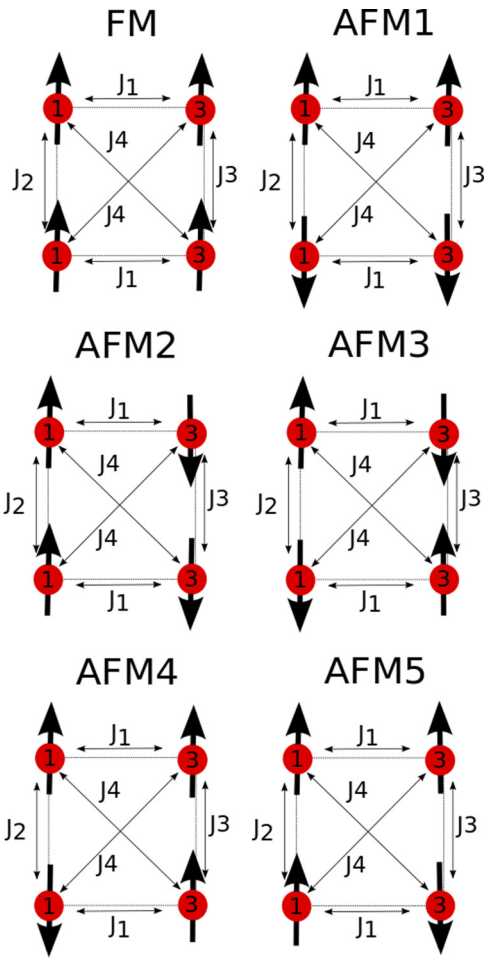

FIG. 8. Ferromagnetic and antiferromagnetic configurations of the 2_vac_D in the plane of O-vacancies. The spin direction of each Co is depicted with arrows. The exchange interactions are labeled with J_1, J_2, J_3, and J_4. The numbers inside the red circles represent the modulus of the magnetization of each Co atom (1 and 3 μ_B) in the corresponding ionic limit.

TABLE I. Energy of the whole unit cell (12 Co atoms) for the different magnetic configurations. They are all referred to the E_{FM}.

	Energy (eV)
E_{FM}	0.0
E_{AFM1}	2.1
E_{AFM2}	0.5
E_{AFM3}	2.2
E_{AFM4}	1.9
E_{AFM5}	2.2

TABLE II. Energies (in eV) for the different configurations at different values of U. The zero of energies is represented by the configuration without vacancies. It can be observed that configuration 2_vac_D is a robust ground state in a wide range of values of U. It is the only configuration that is stable for $U \geqslant 5.5$ eV.

U (eV)	**4.1**	**5.5**	**6.8**	**8.2**
1_vac_A	5.78	5.40	5.08	5.16
1_vac_B	1.33	0.96	0.66	0.70
2_vac_A	2.29	1.44	0.72	0.87
2_vac_B	2.61	1.60	1.23	1.43
2_vac_C	1.00	−0.16	0.08	0.47
2_vac_D	1.93	**−0.24**	**−0.64**	**−0.41**
2_vac_E	3.13	2.41	2.45	2.90
2_vac_F	1.38	1.10	0.99	1.56
2_vac_G	2.61	1.62	1.33	1.75

We can obtain the value of the different exchange interactions as a function of the energies of the magnetic configurations:

$$J_1 = \frac{E_{\mathrm{AFM2}} + E_{\mathrm{AFM3}} - E_{\mathrm{AFM1}} - E_{\mathrm{FM}}}{24} = 300\ \mathrm{K},$$

$$J_2 = \frac{E_{\mathrm{AFM1}} + E_{\mathrm{AFM3}} + 2(E_{\mathrm{AFM4}} - E_{\mathrm{AFM5}}) - E_{\mathrm{AFM2}} - E_{\mathrm{FM}}}{8} = 4600\ \mathrm{K},$$

$$J_3 = \frac{E_{\mathrm{AFM1}} + E_{\mathrm{AFM3}} - 2(E_{\mathrm{AFM4}} - E_{\mathrm{AFM5}}) - E_{\mathrm{AFM2}} - E_{\mathrm{FM}}}{72} = 730\ \mathrm{K},$$

$$J_4 = \frac{E_{\mathrm{AFM1}} + E_{\mathrm{AFM2}} - E_{\mathrm{AFM3}} - E_{\mathrm{FM}}}{24} = 150\ \mathrm{K}. \quad \text{(A1)}$$

We observe from Eqs. (A1) that all the exchange interactions (J's) are positive, which we have taken as ferromagnetic in our sign convention.

APPENDIX B

Table II shows a summary of all the energetics of the configurations considered as a function of U for four selected values of U. We can see that the only stable solution that includes O-vacancies is the one we have analyzed thoroughly in the paper: configuration 2_vac_D. We see that it is the ground state for a wide range of U values, $U \geqslant 5.5$ eV. The typical U values utilized for this kind of cobaltates in similar calculations are in the range of 6–8 eV [23,38,39]. Thus our calculations show a robust trend indicating that configuration 2_vac_D is indeed the ground state of the system.

[1] U. Lüders, A. Barthélémy, M. Bibes, K. Bouzehouane, S. Fusil, E. Jacquet, J.-P. Contour, J.-F. Bobo, J. Fontcuberta, and A. Fert, Adv. Mater. **18**, 1733 (2006).

[2] D. Zhang, X. Xu, W. Wang, X. Zhang, H. Yang, Y. Wu, C. Ma, and Y. Jiang, Rare Metals **31**, 112 (2012).

[3] M. Cesaria, A. P. Caricato, G. Maruccio, and M. Martino, J. Phys. Conf. Ser. **292**, 012003 (2011).

[4] M. Zhu, Y. Lin, E. W. C. Lo, Q. Wang, Z. Zhao, and W. Xie, Appl. Phys. Lett. **100**, 062406 (2012).

[5] A. Fert, Angew. Chem., Int. Ed. **47**, 5956 (2008).

[6] M. Götte, M. Joppe, and T. Dahm, Sci. Rep. **6**, 36070 (2016).

[7] P. Michetti and P. Recher, Phys. Rev. B **84**, 125438 (2011).

[8] F. Katmis, V. Lauter, F. S. Nogueira, B. A. Assaf, M. E. Jamer, P. Wei, B. Satpati, J. W. Freeland, I. Eremin, D. Heiman, P. Jarillo-Herrero, and J. S. Moodera, Nature (London) **533**, 513 (2016).

[9] M. Señarís-Rodríguez and J. Goodenough, J. Solid State Chem. **116**, 224 (1995).

[10] M. W. Haverkort, Z. Hu, J. C. Cezar, T. Burnus, H. Hartmann, M. Reuther, C. Zobel, T. Lorenz, A. Tanaka, N. B. Brookes, H. H. Hsieh, H.-J. Lin, C. T. Chen, and L. H. Tjeng, Phys. Rev. Lett. **97**, 176405 (2006).

[11] K. Asai, A. Yoneda, O. Yokokura, J. Tranquada, G. Shirane, and K. Kohn, J. Phys. Soc. Jpn. **67**, 290 (1998).

[12] M. Abbate, J. C. Fuggle, A. Fujimori, L. H. Tjeng, C. T. Chen, R. Potze, G. A. Sawatzky, H. Eisaki, and S. Uchida, Phys. Rev. B **47**, 16124 (1993).

[13] G. Maris, Y. Ren, V. Volotchaev, C. Zobel, T. Lorenz, and T. T. M. Palstra, Phys. Rev. B **67**, 224423 (2003).

[14] A. M. Durand, D. P. Belanger, C. H. Booth, F. Ye, S. Chi, J. A. Fernandez-Baca, and M. Bhat, J. Phys.: Condens. Matter **25**, 382203 (2013).

[15] J. F. Afonso and J. Kuneš, Phys. Rev. B **95**, 115131 (2017).

[16] J. Baier, S. Jodlauk, M. Kriener, A. Reichl, C. Zobel, H. Kierspel, A. Freimuth, and T. Lorenz, Phys. Rev. B **71**, 014443 (2005).

[17] J. W. Freeland, J. X. Ma, and J. Shi, Appl. Phys. Lett. **93**, 212501 (2008).

[18] D. Fuchs, E. Arac, C. Pinta, S. Schuppler, R. Schneider, and H. v. Löhneysen, Phys. Rev. B **77**, 014434 (2008).

[19] V. V. Mehta, M. Liberati, F. J. Wong, R. V. Chopdekar, E. Arenholz, and Y. Suzuki, J. Appl. Phys. **105**, 07E503 (2009).

[20] V. V. Mehta, N. Biskup, C. Jenkins, E. Arenholz, M. Varela, and Y. Suzuki, Phys. Rev. B **91**, 144418 (2015).

[21] F. Rivadulla, Z. Bi, E. Bauer, B. Rivas-Murias, J. M. Vila-Fungueiriño, and Q. Jia, Chem. Mater. **25**, 55 (2013).

[22] A. Posadas, M. Berg, H. Seo, A. de Lozanne, A. A. Demkov, D. J. Smith, A. P. Kirk, D. Zhernokletov, and R. M. Wallace, Appl. Phys. Lett. **98**, 053104 (2011).

[23] H. Hsu, P. Blaha, R. M. Wentzcovitch, and C. Leighton, Phys. Rev. B **82**, 100406 (2010).

[24] N. Biškup, J. Salafranca, V. Mehta, M. P. Oxley, Y. Suzuki, S. J. Pennycook, S. T. Pantelides, and M. Varela, Phys. Rev. Lett. **112**, 087202 (2014).

[25] J. Gazquez, W. Luo, M. P. Oxley, M. Prange, M. A. Torija, M. Sharma, C. Leighton, S. T. Pantelides, S. J. Pennycook, and M. Varela, Nano Lett. **11**, 973 (2011).

[26] J. Gazquez, S. Bose, M. Sharma, M. A. Torija, S. J. Pennycook, C. Leighton, and M. Varela, APL Mater. **1**, 012105 (2013).

[27] W. S. Choi, J.-H. Kwon, H. Jeen, J. E. Hamann-Borrero, A. Radi, S. Macke, R. Sutarto, F. He, G. A. Sawatzky, V. Hinkov, M. Kim, and H. N. Lee, Nano Lett. **12**, 4966 (2012).
[28] P. Hohenberg and W. Kohn, Phys. Rev. **136**, B864 (1964).
[29] W. Kohn and L. J. Sham, Phys. Rev. **140**, A1133 (1965).
[30] K. Schwarz and P. Blaha, Comput. Mater. Sci. **28**, 259 (2003).
[31] J. P. Perdew, K. Burke, and M. Ernzerhof, Phys. Rev. Lett. **77**, 3865 (1996).
[32] P. J. Linstrom and W. G. Mallard, J. Chem. Eng. Data **46**, 1059 (2001).
[33] A. Sarantopoulos, E. Ferreiro-Vila, V. Pardo, C. Magén, M. H. Aguirre, and F. Rivadulla, Phys. Rev. Lett. **115**, 166801 (2015).
[34] C. Freysoldt, B. Grabowski, T. Hickel, J. Neugebauer, G. Kresse, A. Janotti, and C. G. Van de Walle, Rev. Mod. Phys. **86**, 253 (2014).
[35] A. Janotti, J. B. Varley, P. Rinke, N. Umezawa, G. Kresse, and C. G. Van de Walle, Phys. Rev. B **81**, 085212 (2010).
[36] S. B. Zhang and J. E. Northrup, Phys. Rev. Lett. **67**, 2339 (1991).
[37] L. Iglesias, A. Sarantopoulos, C. Magén, and F. Rivadulla, Phys. Rev. B **95**, 165138 (2017).
[38] M. Topsakal, C. Leighton, and R. M. Wentzcovitch, J. Appl. Phys. **119**, 244310 (2016).
[39] S. L. Dudarev, G. A. Botton, S. Y. Savrasov, C. J. Humphreys, and A. P. Sutton, Phys. Rev. B **57**, 1505 (1998).